Morphological Response of Vegetated and Urbanized Barrier Islands to Hurricane Ian

Muhammad Hassan Ilyas[1], Ap van Dongeren[1,2], Dano Roelvink[1,2], Ellen Quataert[2], Christopher Daly[3]

[1]Coastal and Urban Risk and Resilience Department, IHE Delft Institute for Water Education, Delft, 2611 AX, The Netherlands
[2]Applied Morphodynamics Department, Deltares, Delft, 2629 HV, The Netherlands
[3]The Water School, Florida Gulf Coast University, Fort Myers, Florida, 33965, United States of America

Correspondence to: M. Hassan Ilyas (ilyasmhassan6@gmail.com)

Abstract. Barrier islands are vulnerable to extreme storm events which cause erosion and deposition of sediment. These morphological changes pose risks to both the built environment and natural habitats but are also affected by them. This study investigates the morphological impacts of Hurricane Ian (2022) on two barrier islands along Florida's Gulf Coast: the urbanized Fort Myers Beach, and Lovers Key, a naturally vegetated island and State Park. Using high-resolution pre- and post-storm topo-bathymetric datasets, we quantify patterns of erosion, sediment deposition and dune crest change. In addition, we investigated the morphological response of the developed and natural barrier islands by integrating spatially varying land cover data into the numerical model XBeach. Results show that the built environment on Fort Myers Beach significantly affects sediment transport pathways, causing localized erosion and deposition patterns distinct from those observed on the vegetated Lovers Key Island where dune crest lowering, landward migration, and storm-induced breach were prominent. Model simulations that incorporated detailed spatial variability of vegetation and built environment, replicated observed morphological changes with reasonable Brier Skill Scores, including the location of breach formation. Sensitivity analyses demonstrated that relatively small changes in roughness coefficient, wave skewness and asymmetry factor, morphological acceleration factor, and boundary water levels influence erosion intensity and sediment deposition patterns. Additionally, introducing supplemental vegetation patches in the model showed less dune erosion on vegetated barrier island, indicating that revegetation of islands may be beneficial. The findings provide insights into the complex interplay between storm forcing, land cover variability, and barrier island morphodynamics, and emphasize the importance of incorporating detailed land use and vegetation data in morphodynamic models to better assess barrier island responses to future storms under evolving climatic conditions, ultimately aiding efforts to enhance coastal resilience and adaptive management.

1 Introduction

Barrier islands are integral components of sandy coastlines, covering 10% of the world's coastlines (Stutz & Pilkey, 2011). They provide space for natural habitat, support livelihoods and recreation, and act as critical buffers that reduce backshore flooding during extreme events (Nordstrom, 2000). Storms continually reshape barrier islands by driving large-scale sediment transport through both landward and seaward processes under distinct impact regimes (Pardo-Pascual et al., 2014; Sallenger, 2000) causing berm erosion, dune crest lowering, overwash and breaching. Storms change the shoreline orientation and position (Almeida et al., 2012) as waves and storm surges erode and redistribute sediment (Harris et al., 2011; Lavaud et al., 2020). Storm surges transport sediments landward, forming overwash deposits and driving barrier island migration. However, in highly urbanized settings, the built environment alters overwash processes, disrupts the islands' natural ability to migrate, reorient and recover, and increases the risk of potential damages (Jiménez et al., 2011; Lazarus et al., 2021). Barrier islands are becoming increasingly vulnerable not only as human occupation intensifies, but also as extreme events become more frequent and sea level rise accelerates (IPCC, 2018; Jiménez et al., 2011). During the latter half of the 20th century, global mean sea level rose at about 2.5 mm/year and in recent decades has accelerated to about 3.9 mm/year (Brooks et al., 2017; IPCC, 2021). Projections for the coming decades indicate that even modest increases in sea level will amplify storm impacts, leading to extensive inundation and substantial morphological alterations of low-lying coastal landscapes and sandy barrier systems (FitzGerald et al., 2008; Tebaldi et al., 2012). Understanding the rapid morphological changes in the presence of vegetation and built environment resulting from storm events is essential not only for effectively managing the coastline but also for developing and implementing mitigation strategies to reduce future risk (Harley et al., 2017; Jiménez et al., 2018).

Morphodynamic models such as XBeach can simulate storm-induced coastal change by explicitly resolving hydrodynamic and sediment transport processes as well as morphological updating (McCall et al., 2010; Roelvink et al., 2009; Sherwood et al., 2022). In XBeach, the effects of vegetation and other land cover types (e.g., vegetated dunes, mangroves, buildings, or engineered terrain) can be represented by a bed roughness according to Land Use and Land Cover (LULC) data. Roelvink et al. (2009), McCall et al. (2010), and Lindemer et al. (2010) used a constant Chezy bed roughness across the entire model domain, regardless of vegetation presence. De Vet et al. (2015), Passeri et al. (2018), and Van Der Lugt et al. (2019) advanced these approaches by incorporating spatially variable roughness and vegetation dynamics, such as applying different Manning's coefficients for vegetated and non-vegetated areas or implementing dynamic roughness modules that adjust in response to changes in vegetation cover during extreme storms, resulting in improved predictions of storm-driven morphological change. Note that the increased Manning's coefficients directly affect the hydrodynamics but only indirectly, through reduced velocities, affect the sediment transport and morphology.

In this study, we implemented XBeach area models to simulate the impact of Hurricane Ian (2022) on two Florida barrier islands, with a focus on the natural Lovers Key and the urbanized Fort Myers Beach. The study emphasizes how spatial variability in LULC influences morphological changes during extreme storm events. We employed different LULC datasets

to assess the effects of varying land cover configurations on sedimentation and erosion patterns and dune crest change, hereafter referred to as Scenarios. This study also investigated the sensitivity of model outputs to key parameters including

65 wave skewness and asymmetry (*facua*), the morphological acceleration factor (*morfac*), and forcing conditions such as wave height and water levels. Additionally, the impact of supplemental vegetation on the Lovers Key's morphodynamics was evaluated. Section 2 presents the study area and data used, Section 3 describes the methodology and evaluation metrics, Section 4 reports the results, and Sections 5 and 6 provide discussion and conclusions.

2 Study Area and Data Availability

70 Hurricane Ian originated from a tropical wave that emerged off West coast of Africa. It intensified over the Gulf of Mexico and made landfall as Category 4 in Lee County, Florida on 28 September 2022. Our study focuses on Fort Myers Beach, on Estero Island, a low lying and densely developed barrier island bounded by San Carlos Bay to the north and Big Carlos Pass to the south, and on nearby Lovers Key on the Lovers Key State Park (Fig. 1). On Estero Island, more than 2,400 structures were impacted, with damage to heavily affected buildings estimated to exceed USD 200 million (Hauptman et al., 2024).

75 Lovers Key comprises four interconnected barrier islands: Lovers Key, Inner Key, Long Key, and Black Island. It is bounded by Big Carlos Pass to the north and New Pass to the south and contains relatively natural beach dune and back barrier ecosystems. After Hurricane Charley in 2004, dune and vegetation restoration through nourishment and planting was undertaken, with major works completed by 2014 (FDEP, 2005). During Ian, storm surge inundated Lovers Key, driving substantial morphological change, including a breach near the northern end by the bridge and widespread dune lowering.

80 The data sources for topo-bathymetry include data from the National Oceanic and Atmospheric Administration (NOAA), referred to as "NOAA Pre-Ian" and "NOAA Post-Ian" rasterized topo-bathymetric Digital Elevation Models (DEMs). The NOAA Pre-Ian (OCM Partners, 2025a) was collected between May and June 2022, and the NOAA Post-Ian (OCM Partners, 2025b) in November 2022 with a 1-meter grid resolution. The NOAA Post-Ian has a smaller spatial coverage compared to the pre-storm dataset because the Light Detection and Ranging (LiDAR) could not penetrate deep below the water surface

85 due to the high turbidity following the hurricane. Additionally, an in-situ dataset is provided by Coastal Engineering Consultants (CEC). These transects, referred to as "CEC Pre-Ian" and "CEC Post-Ian", were surveyed before and after Hurricane Ian in June–July 2022 and October–November 2022, respectively. In total, 57 transects were surveyed, with 43 transects on Fort Myers Beach (Transect No. 1 to Transect No. 43) and 14 transects on Lovers Key (Transect No. 44 to Transect No. 57). The survey methodology used by CEC involved high-precision Global Positioning System (GPS) and total

90 station measurements, ensuring accurate elevation data collection along each transect. An additional dataset with a smaller spatial extent compared to the NOAA and CEC datasets is provided by Florida Gulf Coast University (FGCU), which conducted pre- and post-Hurricane Ian LiDAR surveys for Lovers Key in June 2022 and October 2022, respectively, and are referred to as "FGCU Pre-Ian" and "FGCU Post-Ian".

Two main sources of LULC data are available for the study areas. The first is a nationally standardized land cover dataset derived from the NOAA 2022 satellite imagery, which provides 1-meter resolution coverage of coastal intertidal areas, wetlands, and adjacent uplands (Office for Coastal Management, 2025a, 2025b). The second data source is from the National Oceanographic Partnership Program (NOPP), which provides a fused high-resolution LULC dataset that integrates satellite imagery, with spatial resolutions ranging from 1 to 30 meters (NOPP, 2021).
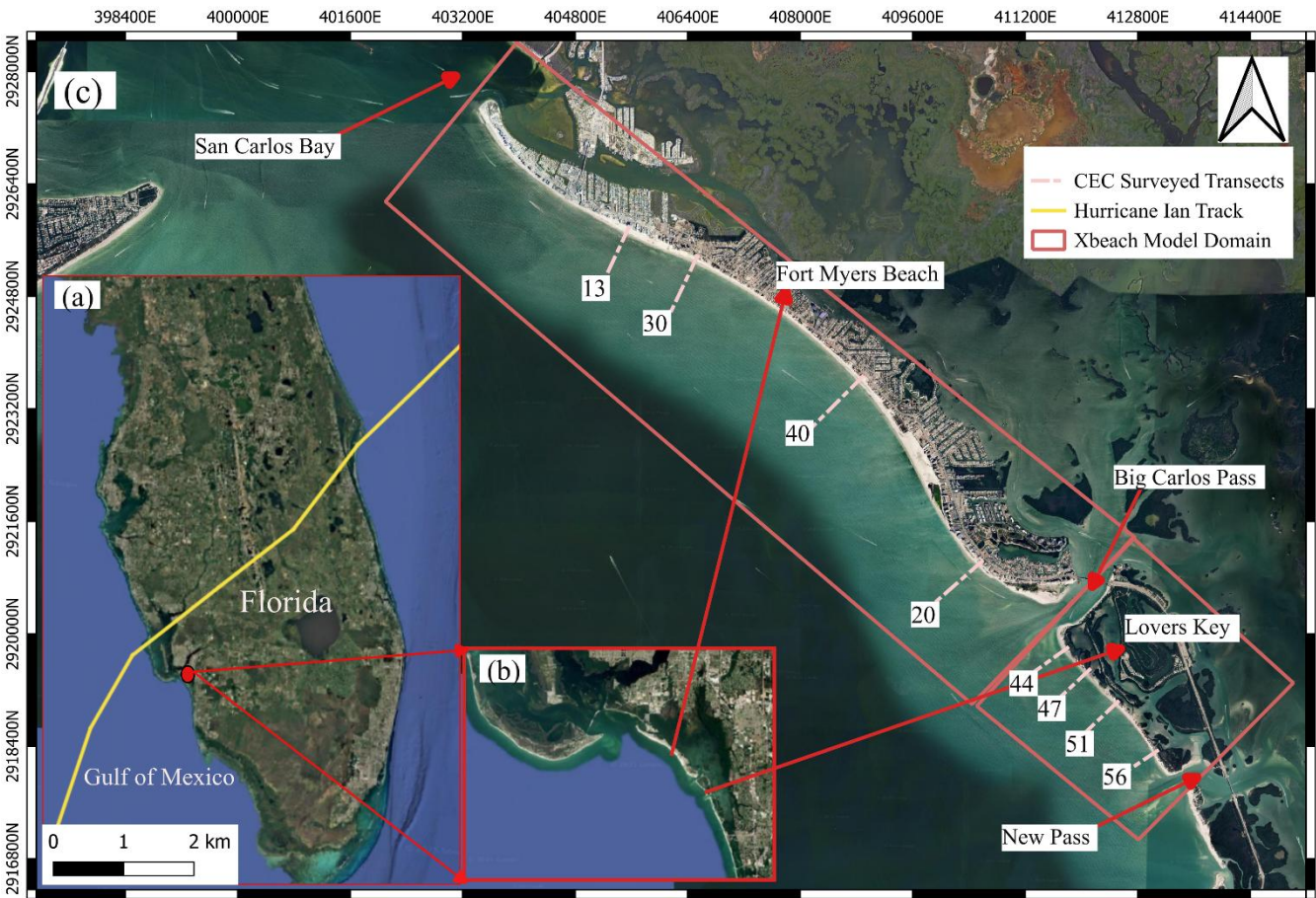
Figure 1 Study area maps showing (a) Florida and the track of Hurricane Ian (yellow line), (b) the focus sudy area along the southwest coast of Florida, and (c) detailed views of Fort Myers Beach and Lovers Key with surrounding passes (Big Carlos Pass, New Pass) and San Carlos Bay, including CEC surveyed transects (dashed lines) and XBeach model domains (red rectangles) (© Google Earth).

3 Methodology

3.1 Model Setup

In this study, two 2DH XBeach area models (version 1.24.6057-Halloween Beta release) were set up for Lovers Key and Fort Myers Beach, both configured in surfbeat mode. A morphological acceleration factor *(morfac)* of 5 was applied to reduce computational expense, and all other parameters remained at their default settings. A uniform rectangular grid with 2-meter spacing in the cross-shore direction and 5-metre spacing alongshore was chosen for both domains, as shown in Fig. 1. The grid was extended alongshore to the channels around the barrier heads, to be able to include the hydrodynamics that may affect morphological change on the island heads during Hurricane Ian.

3.2 Bathymetry

The bathymetry was generated by combining the NOAA Pre-Ian DEM, which extends to depths of up to 7 meters, with the 1-meter-resolution Continuously Updated Digital Elevation Model (CUDEM) dataset (NOAA, 2018) to provide coverage of deeper waters. Considering the Gulf of Mexico's shallow offshore bathymetry, the model domain was truncated at 9 meters below NAVD88. Beyond this depth, the bathymetry was extended seaward to 25 meters on a gentle slope of 1:50, minimizing numerical instabilities at the open boundary.

3.3 Boundary Forcings

The models were forced with time-varying wave and water level boundaries which were derived from the surge (SFINCS) and wave (HurryWave) models using COAMPS-TC (Doyle et al., 2014) meteorological input. The wave conditions shown in Fig. 2a were imposed at the offshore boundary for each site. Neumann lateral boundary conditions were applied at the seaward and landward boundaries to maintain constant water levels, with two tidal signals specified at the offshore (sea) and landward (land) boundaries, as illustrated in Fig. 2b. A simulation duration of 30 hours was specified to capture the rise and fall of the storm.
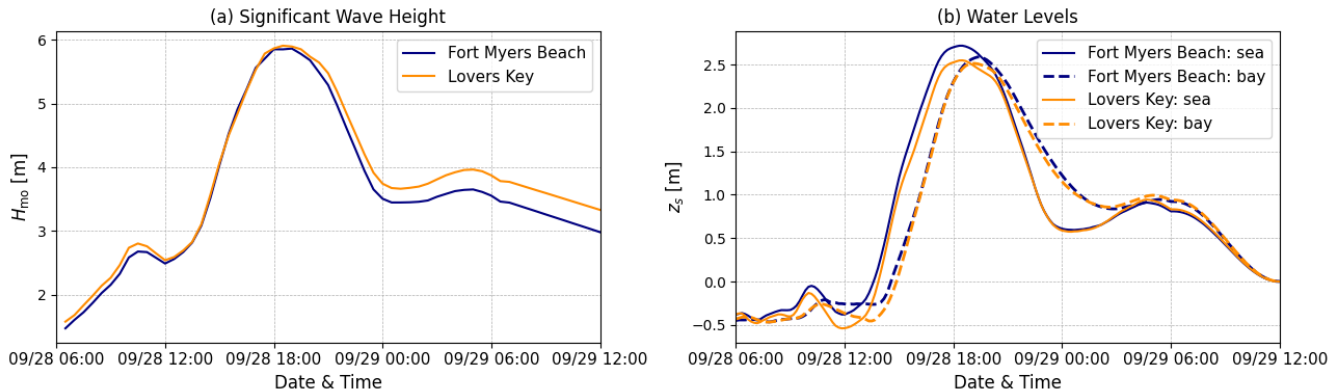
Figure 2 Time series of (a) Significant Wave Height (H_{mo}) and (b) Water Levels (z_s) at Lovers Key (orange lines) and Fort Myers (blue lines) Beach during Hurricane Ian. Solid lines indicate boundary locations on the Gulf side, while dashed lines indicate the
130 **bay side.**

3.4 Land Use Land Cover Scenarios

To evaluate the modelled morphological change for different LULC data sources, we defined three baseline Manning's roughness scenarios to represent the influence of vegetation and built environment. The built environment (including buildings, roads, and warehouses) was represented based on the digital terrain model, which excludes above-ground raised
135 topography (i.e., increased bed level). Their effects on hydrodynamics and sediment transport were captured through higher Manning's roughness values, as described below.

- Scenario 1 (S1) applies a uniform Manning's roughness coefficient of 0.02 to simulate a sandy bed and serves as a reference case.
- Scenario 2 (S2), shown for Fort Myers Beach in Fig. 3a and for Lovers Key in Fig. 3c, uses LULC data from the
140 NOPP project, originally consisting of 23 classes, which were reclassified into four categories based on Mattocks & Forbes, (2008) as reported by (Salgado, 2023): primary vegetation with a roughness of 0.04, secondary vegetation with 0.05, sandy bed with 0.02, and built environment with 0.10.
- Scenario 3 (S3), shown for Fort Myers Beach in Fig. 3b and for Lovers Key in Fig. 3d, uses NOAA canopy cover and impervious surface data, assigning roughness values of 0.04 for scrub or shrub areas (primary vegetation), 0.05
145 for upland trees (secondary vegetation), and 0.10 for built environment.

Figure 3 illustrates the spatial distribution of land cover classifications used in Scenarios 2 and 3 for both study sites. For Fort Myers Beach, the NOAA dataset (Scenario 3) provides a more recent and higher-resolution (1 m) representation of the built environment, capturing finer details of built features such as roads and impervious surfaces. In contrast, the NOPP dataset (Scenario 2) has a resolution (1–30 m) and depicts a denser distribution of non-erodible areas, resulting in more
150 extensive coverage of urban surfaces. For Lovers Key, several patches of primary vegetation along the back-barrier and foredune zones are classified as secondary vegetation in Scenario 3, highlighting differences in vegetation classification between the two datasets.
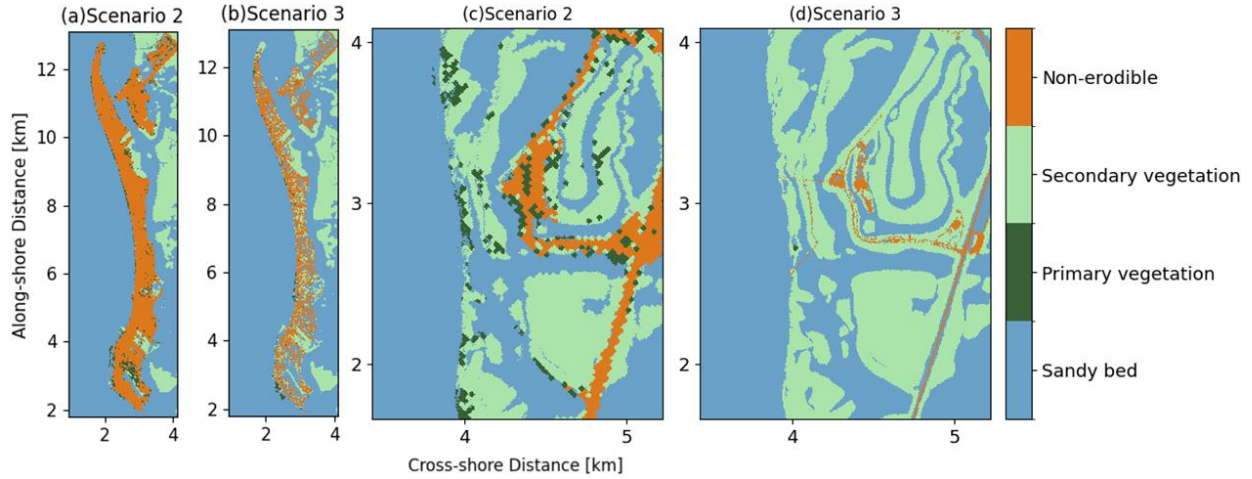
155 **Figure 3 Spatial Land Use Land Cover classification maps for Scenarios 2 (NOPP dataset) and Scenario 3 (NOAA dataset): (a) and (b) Fort Myers Beach, (c) and (d) Lovers Key. Manning's n values are 0.02 for sandy bed, 0.04 for primary vegetation, 0.05 for secondary vegetation, and 0.1 for non-erodible surfaces.**

3.5 Evaluation Metrics

The performance of the model was evaluated using the bias and Brier Skill Score (BSS), which were calculated following

160 Equations 1 and 2.

$$Bias = \frac{1}{N} \sum_{i=1}^{N} (z_{b,modelled} - z_{b,measured}) \tag{1}$$

$$BSS = 1 - \frac{\frac{I}{N}\sum_{i=1}^{N}(z_{b,modelled} - z_{b,measured})^2}{\frac{I}{N}\sum_{i=1}^{N}(z_{b,inital} - z_{b,measured})^2} \tag{2}$$

Where $z_{b,modelled}$ is the predicted bed level, $z_{b,measured}$ is the post-Ian observed bed level, $z_{b,inital}$ is the pre-Ian bed level and N is the total number of points. BSS values were classified as Excellent (0.8–1.0), Good (0.6–0.8), Reasonable

165 (0.3–0.6), Bad (0.0–0.3), and Poor (<0.0), following (Van Rijn et al., 2003)

For Lovers Key, the change in dune crest elevation was evaluated by plotting transects perpendicular to the coastline, extending approximately 200 meters inland to intersect the primary dune. The dune crest is defined as the first maximum elevation along each transect (Equation 3), and crest shift is defined as the horizontal displacement of the dune crest relative to its initial position, as predicted or observed (Equation 4):

170 $$z_{crest} = max(z_b (x, y)) \tag{3}$$

$$\Delta c = z_{crest,pmodelled} - z_{crest,initial} \tag{4}$$

where x and y are the coordinates corresponding to the maximum elevation.

4 Results

4.1 Morphological Response of Lovers Key

175   At Lovers Key, in Scenario 1, the all-sand bed roughness approach (Fig. 4b) fails to reproduce the observed post-hurricane topography (Fig. 4a). Erosion is significantly overestimated, leading to overprediction of sediment deposition landward and overprediction of the breach extent (BSS = -2.96). In Scenario 2 (Fig. 4c), the inclusion of increased Manning's n values in vegetated areas introduces flow resistance, leading to less exaggerated erosion and more localized sedimentation patterns which agrees better with the observations (BSS = 0.38). Scenario 3, based on NOAA LULC data, (Fig. 4d) yields a bed-level

180   distribution slightly more consistent with the observations (BSS = 0.40), capturing improved sediment retention and a breach width that aligns more closely with post-Ian observed data. For the Lovers Key model, the inclusion of vegetation, represented by locally increased bed friction, improves morphodynamic predictions, consistent with the conclusions of Van Der Lugt et al., (2019). The application of the two different LULC datasets in Scenario 2 and Scenario 3 do not result in significant different sedimentation and erosion patterns, despite the differences in land use classification (Fig 3c and d).

185
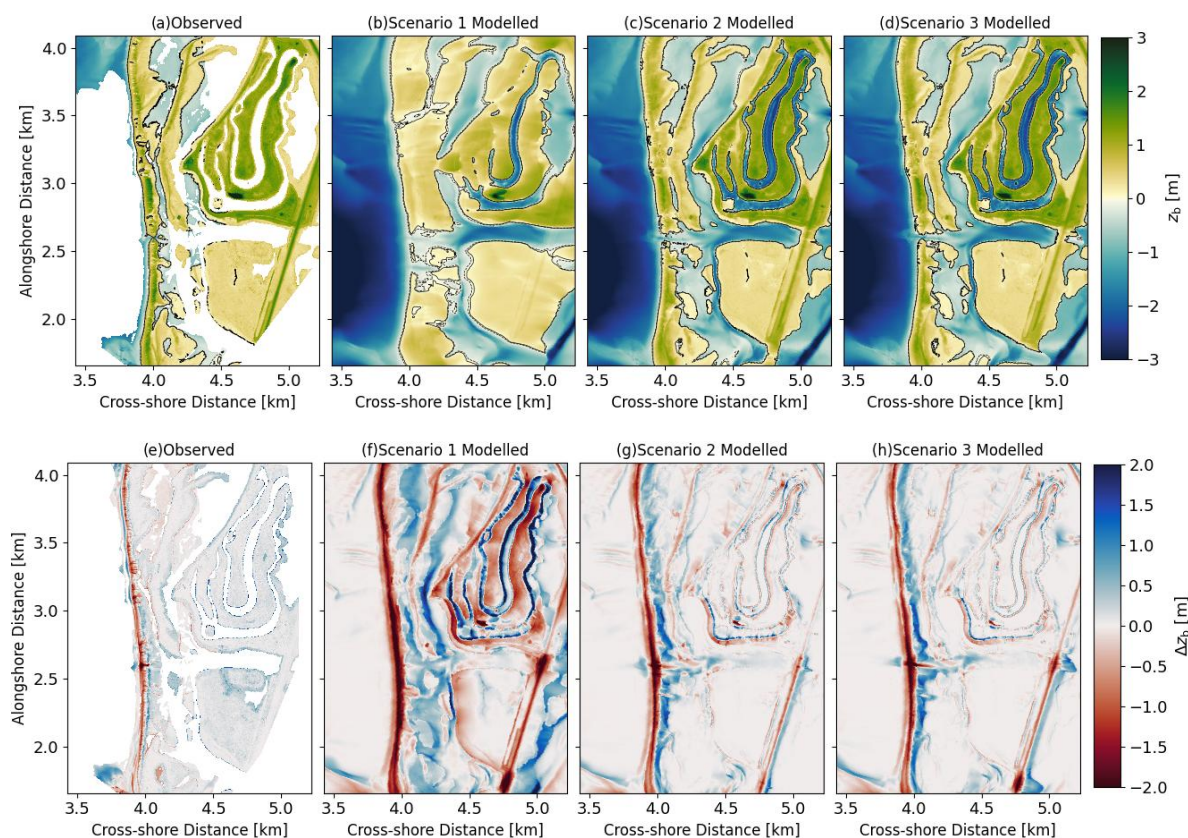
Figure 4 Observed and computed post-Ian bed level and sedimentation and erosion patterns for Lovers Key. (a) NOAA observations; (b) XBeach modelled Scenario 1 with uniform sandy roughness; (c) Scenario 2 based on the NOPP LULC dataset; and (d) Scenario 3 based on the NOAA LULC dataset. The bottom row shows sedimentation and erosion plots for (e) observed, (f)
190 **Scenario 1, (g) Scenario 2, and (h) Scenario 3.**

4.1.1 Dune Crest Change

The comparison of modelled and observed alongshore dune crest elevation change (Fig. 5a) and cross-shore crest shift (Fig. 5b) highlights differences across modelled scenarios. All scenarios show dune crest lowering, but the magnitude of this change varies significantly. Scenario 1 overestimates crest lowering, with an average of 1.25 m, which is greater than the observed 0.35 m (NOAA) and 0.43 m (FGCU). In contrast, Scenario 3, with an average crest lowering of 0.44 m, closely matches the NOAA observations, while Scenario 2 predicts an average lowering of 0.57 m. The reduced erosion in Scenario 3 can be attributed to the higher proportion of secondary vegetated areas in the NOAA LULC dataset, which increases local bed roughness in the model (Fig. 3) and demonstrates that incorporating spatially varying bed friction improves dune erosion prediction (Van Der Lugt et al., 2019; Van Puijenbroek et al., 2017). Alongshore patterns reveal further differences, with NOAA and FGCU data showing alternating zones of moderate lowering and stability between 0.5 and 1.0 km, while Scenario 1 smooths out this variability and consistently predicts excessive lowering; Scenario 2 and Scenario 3 better reproduce the alongshore variability but overestimate the lowering on the northern side of the breach (x ≈ 0.65 km), where sediment transported into the breach was likely deposited by waning flows over time. Similarly, for crest shift, Scenario 3 provides the closest match to observations (30.05 m) compared to 19.87 m for NOAA and 20.10 m for FGCU. However, the alongshore variability in observed cross-shore crest shifts, with landward displacement peaking near the breach, is only partially reproduced, while Scenario 1 exaggerates this shift at 43.23 m and Scenario 2 predicts 32.61 m.
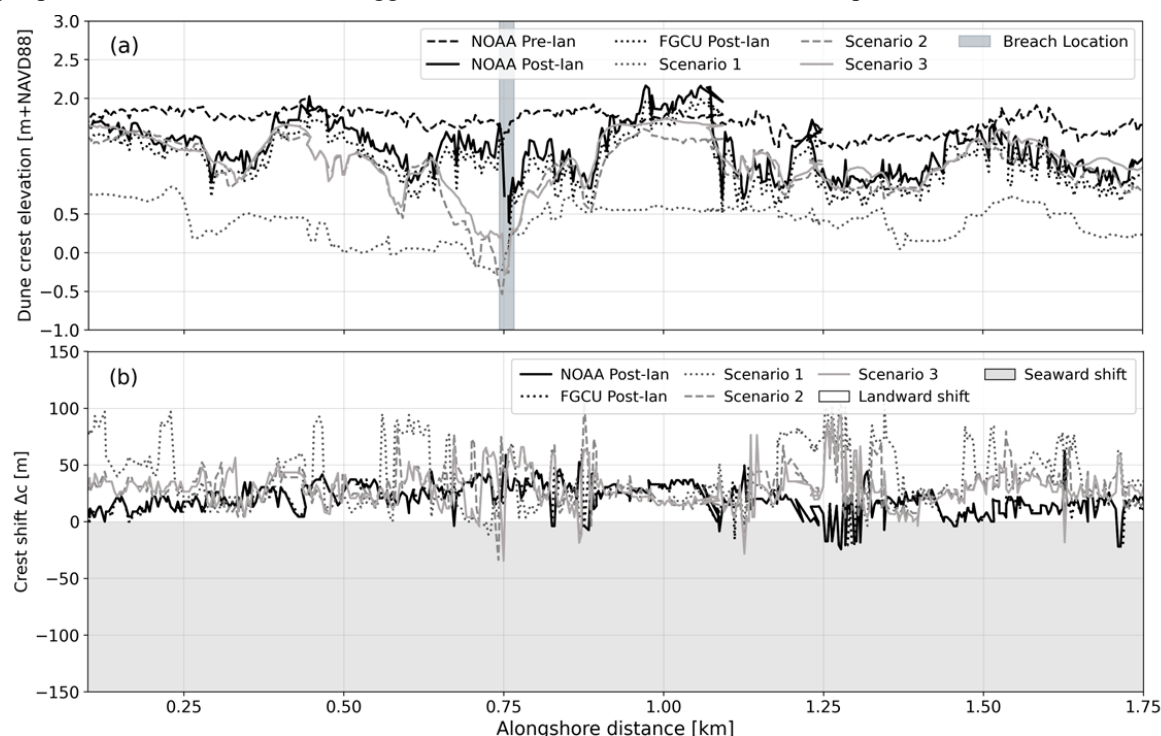
Figure 5 (a) Dune crest elevation changes versus alongshore distance and (b) horizontal dune crest shift at Lovers Key for observed data (NOAA and FGCU) and XBeach modelled Scenarios 1, 2, and 3 (described in Fig. 4).

4.1.2 Model Versus Observed Cross-shore Profiles

Besides comparing to remotely sensed spatial patterns, we have also evaluated the model against in-situ observations, as shown by the CEC surveyed transects outlined in Fig. 1. In Transect 44 (Fig. 6a), the pre-storm dune crest elevation was approximately 1.75 m (at x = 425 m), but post-storm it was reduced to 1.15 m. In Scenario 1, the dune was fully eroded and sand was deposited between x = 100–300 m, while Scenario 2 and Scenario 3 capture the post-storm dune crest but show a slight overestimation of dune erosion, with the excess sediment deposited landward between x = 300–400 m. Similar onshore sediment transport patterns were observed for Transect 47 (Fig. 6b), Transect 51 (Fig. 6c), and Transect 56 (Fig. 6d). In Transect 47, which passes through dense vegetation cover, the crest remained stable; Scenario 2 and Scenario 3 showed similar dune crest positions, with deviations of approximately –0.5 m compared to the observed profile, while in Scenario 1 the dune was washed away entirely. In Transect 51, the crest migrated inland to x = 350 m, and XBeach modelled the dune crest at a similar horizontal position to the post-Ian observations, as was also the case for Transect 47. In Transect 56, the dune crest dropped by more than 0.5 m, and in the modelled Scenarios 2 and 3, the eroded sediment was deposited further inland. Across all modelled scenarios, dune erosion and inland deposition was greater than in the observed profiles Overall, among all transects, Scenario 2 and Scenario 3 matched the observed dune crest more closely than Scenario 1, whereas in Scenario 1 dune crest is fully eroded.
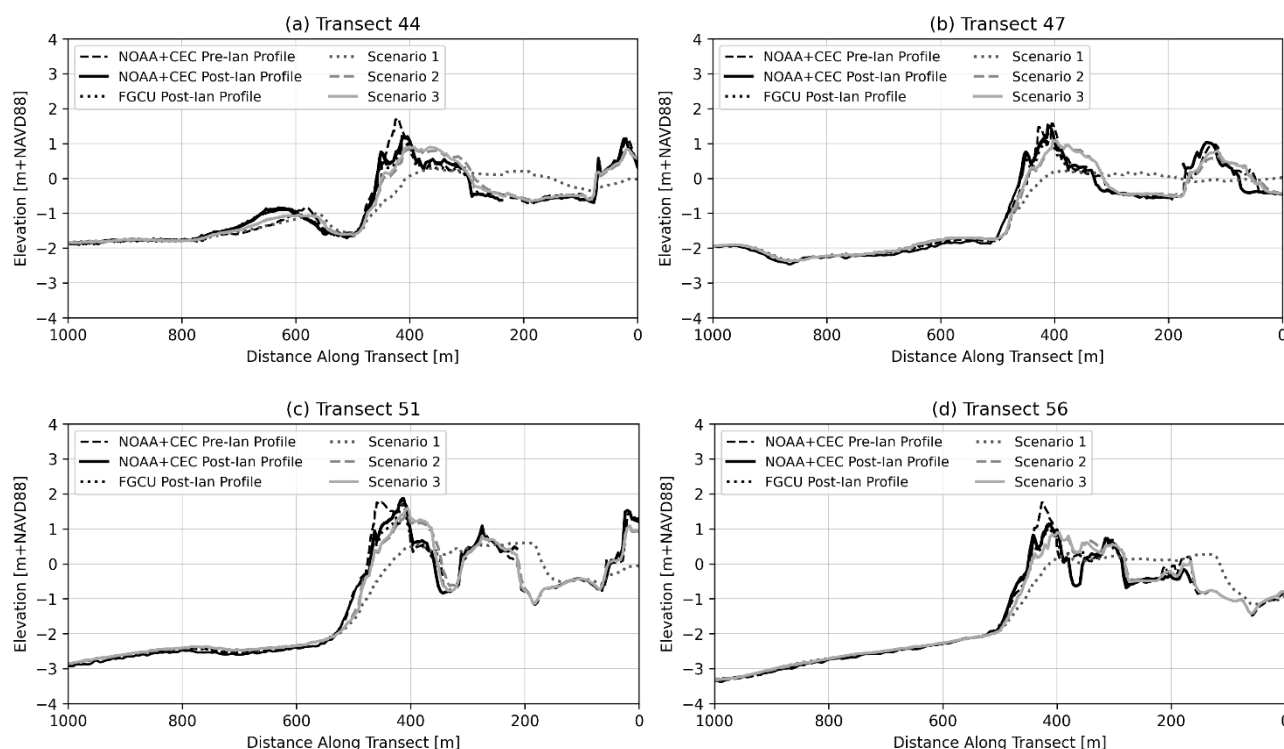
Figure 6 Comparison of XBeach modelled Scenarios 1 (dotted line), 2 (dashed line), and 3 (solid line) (described in Fig. 4) with observed data at Transects 44, 47, 51, and 56 (shown in Fig. 1) at Lovers Key.

4.2 Morphological Response of Fort Myers Beach

230   Fort Myers Beach's built environment strongly modulates sediment dynamics during hurricane Ian, producing a continuous erosion band along the beach and landward overwash deposits (Fig. 7a). Observed bed elevations following the storm were compared with XBeach model outputs under the three scenarios, as shown in Fig. 7b, c and d. Scenario 1 predicts almost complete sediment loss, as it lacks the spatial variability provided by vegetation and hard structures that resist flow, resulting in widespread erosion (BSS=–0.58). This scenario highlights that without incorporating spatial roughness, the model cannot

235   reproduce depositional features or localized variability, instead predicting uniform erosion across the barrier island. Scenario 2 applies a dense built environment bed roughness across the barrier island, which also maps some vegetated areas as urbanized, including both the northern end near Bowditch Park and the southern tip of the island (Fig. 3a). This results in impeded incoming flow and affecting the sediment transport, with BSS=0.42. Although this improves predictive skill compared to Scenario 1, the oversimplified classification reduces accuracy by artificially blocking areas that should allow

240   storm-driven flows. Scenario 3 combines detailed vegetation mapping with a hard-structure layer at higher resolution compared to Scenario 2, better matching observed deposition and erosion patterns with a BSS=0.45. A noticeable effect of urbanization was the formation of overwash with reduced deposition immediately landward of buildings or roads and the accumulation of sand on their seaward side, with urbanized areas also experiencing overwash deposits and local scouring, highlighting how built environment influences flow and sediment deposition (Hapke et al., 2015; Houser et al., 2008). This

245   contrasts with Lovers Key, where sand was transported more landward and the dune crest migrated landward, and vegetation led to less erosion, as shown by Scenario 3 based on NOAA data compared to Scenario 1, which was based only on a sandy bed approach. The summary of Brier Skill Scores and bias for Scenarios 1,2, and 3 for Lovers Key and Fort Myers Beach is presented in Table 1.

250   **Table 1 Brier Skill Scores (BSS) and bias values for Lovers Key and Fort Myers Beach for Scenarios 1, 2, and 3.**

Scenario	Lovers Key		Fort Myers Beach	
	BSS	Bias (m)	BSS	Bias (m)
Scenario 1	-2.96	-0.247	-0.58	-0.169
Scenario 2	0.38	-0.065	0.42	-0.082
Scenario 3	0.40	-0.068	0.45	-0.079
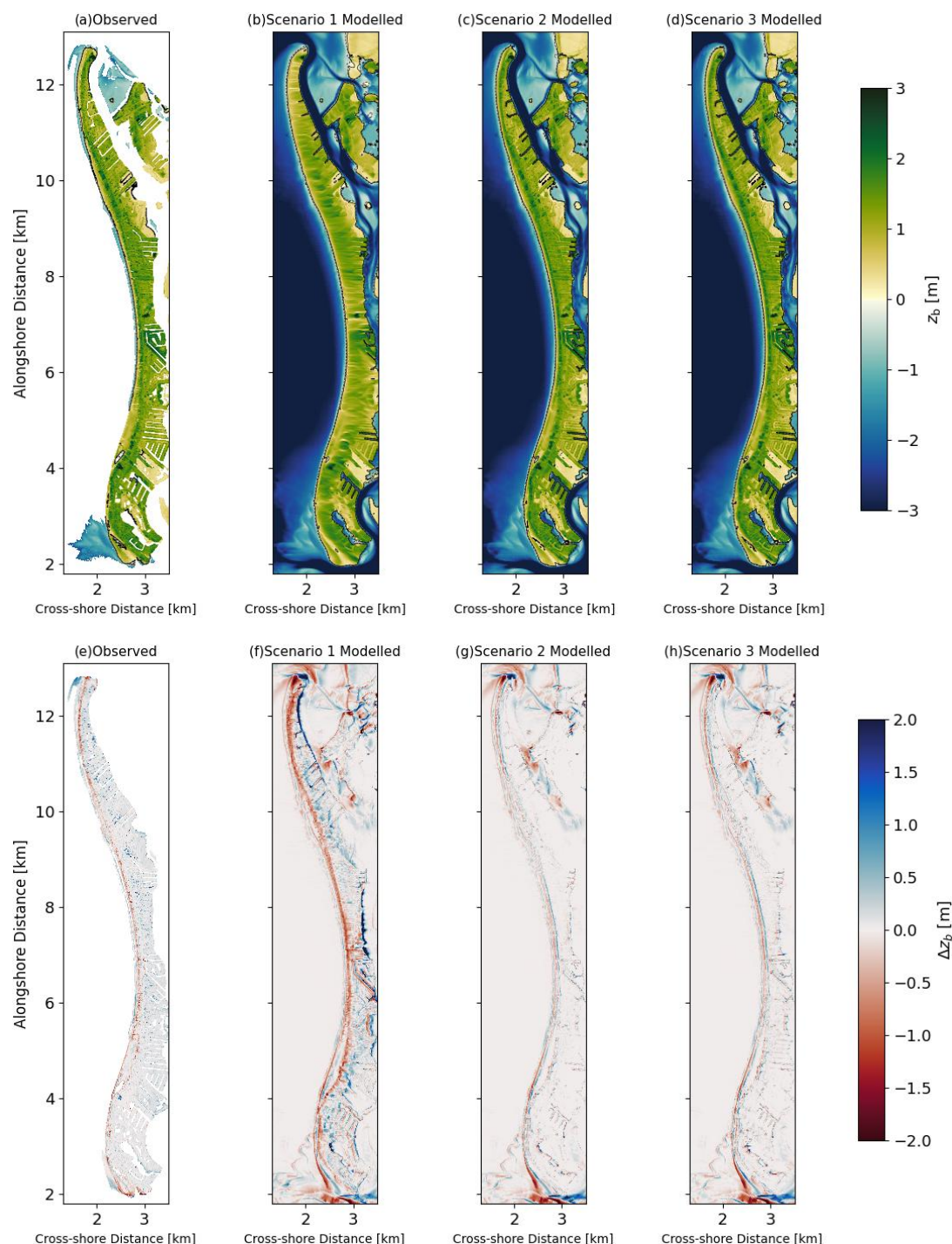
Figure 7 Observed and computed post-Ian bed level and sedimentation and erosion patterns for Fort Myers Beach. (a) NOAA observations; (b) XBeach modelled Scenario 1 with uniform sandy roughness; (c) Scenario 2 based on the NOPP LULC dataset; and (d) Scenario 3 based on the NOAA LULC dataset. The bottom row shows sedimentation and erosion plots for (e) observed, (f) Scenario 1, (g) Scenario 2, and (h) Scenario 3.

Model Versus Observed Cross-shore Profiles

260 Similarly to Lovers Key, in addition to comparing with remotely sensed spatial patterns, we have also evaluated the model against in-situ observations from the CEC surveyed transects (Transects 13, 20, 31, and 40) shown in Fig. 1. In Transect 13 (Fig. 8a), the post-storm profile shows offshore sand accumulation between x = 400–600 m, which is not captured in any of the modelled scenarios. Scenario 1 fails to reproduce this trend, while Scenario 2 shows a small accumulation at x = 380 m. For Transect 20 (Fig. 8b), at the southward end, Scenario 2 and Scenario 3 results align with the post-Ian observed data,

265 albeit with more sand transported landward between x = 200–350 m; both scenarios better predict the morphological change overland. In Transect 31 (Fig. 8c), the post-storm profile also shows offshore sand accumulation between x = 400–600 m, which is not reproduced in any modelled scenario. At approximately x = 250 m, deposition is observed where the transect intersects buildings, leading to localized sediment accumulation. In Transect 40 (Fig. 8d), Scenario 3 follows the post-storm observed profile more closely, particularly between x = 100–300 m. Overall, across all transects, Scenario 1 fails to

270 reproduce observed patterns, highlighting the importance of incorporating bed roughness based on varying built environment and vegetation into the model to accurately simulate storm-driven morphodynamic response.
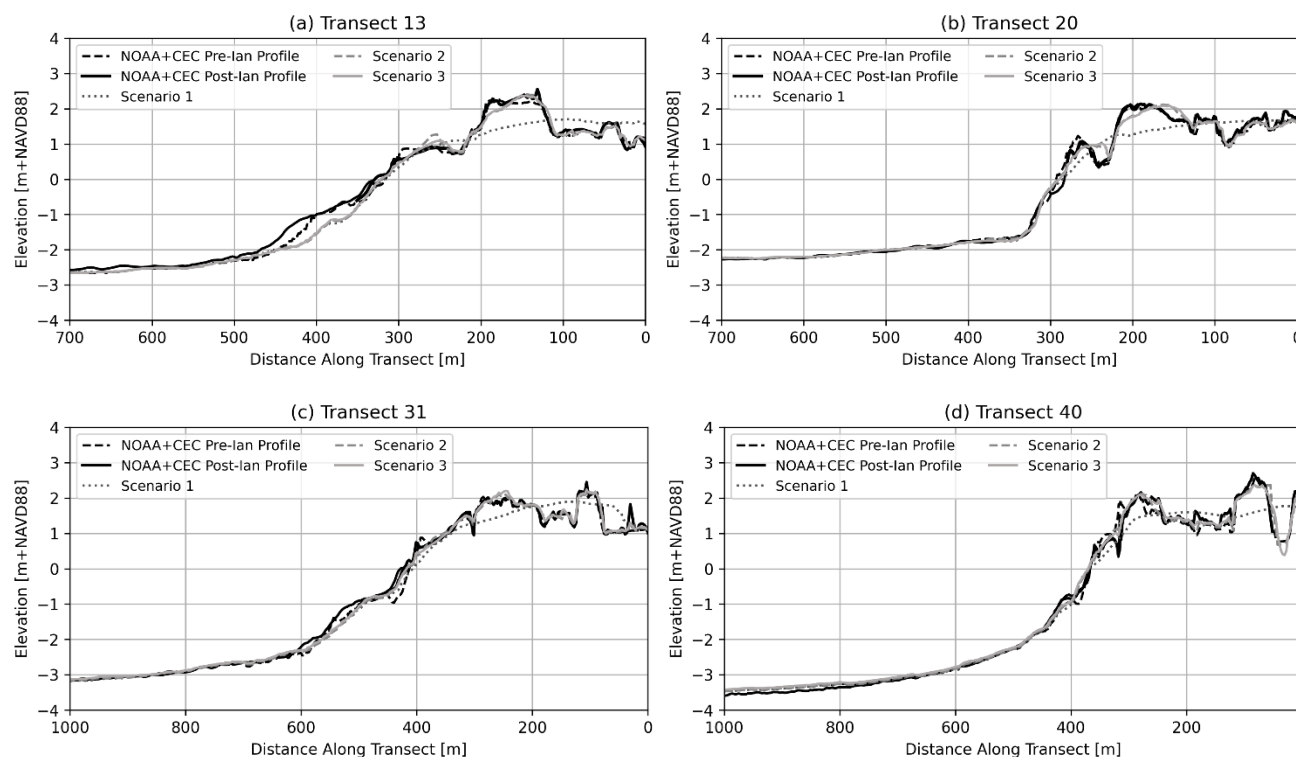
Figure 8 Comparison of XBeach modelled Scenarios 1 (dotted line), 2 (dashed line), and 3 (solid line) (described in Fig. 4) with
275 **observed data at Transects 13, 20, 31, and 40 (shown in Fig. 1) at Fort Myers Beach.**

5 Discussion

In this section, we discuss the sensitivity of different XBeach input parameters and forcing conditions that affect morphodynamic response, as well as the role of supplemental vegetation. We used default parameter settings and tested

280 sensitivity to Manning's *n* value, wave skewness and asymmetry (*facua*), morphological acceleration factor (*morfac*), water levels, and offshore wave heights. In addition, we investigated how supplemental vegetation influences bed-level changes under similar forcing conditions, as discussed in the sections below.

5.1 Sensitivity Analysis of Morphological Response to Model Parameters

A sensitivity analysis was conducted to evaluate how XBeach input parameters and forcing conditions influence

285 morphodynamic predictions, with detailed results summarized in Appendix A. Overall, changes in Manning's *n* and *facua* values altered erosion and sedimentation patterns. Reducing Manning's *n* led to amplified dune erosion and enhanced deposition farther inland, while increasing Manning's *n* increased bottom friction, resulting in lower dune erosion and less sediment accumulation landward. Reducing *facua* resulted in reduced erosion and less pronounced back-barrier deposition, whereas increasing *facua* amplified wave skewness and asymmetry, leading to more erosion seaward of the dune toe and a

290 broader inland deposition zone. For the morphological acceleration factor, *morfac=*3 produced results very similar to *morfac=*5, whereas *morfac=*10 generated unrealistic morphodynamic responses despite reducing computational time. Boundary-condition tests were included to account for uncertainty in observed or forecast storm-surge and wave data, with results showing that water-level variation had a stronger impact than wave height.

The modelling approach applied in this study for South-West Florida is transferable to barrier-island locations worldwide.

295 This study has shown that the critical input and forcing data required to obtain meaningful results are high-resolution topo-bathymetric data, land-use land-cover (LULC) data, and water levels. The availability of these input data may vary. Other U.S. locations can use the same NOAA sources of input and forcing data sets used here. For other locations, the availability and quality of the input and forcing data may vary, although it is improving. Data for European locations are available through Copernicus databases such as the Copernicus DEM (GLO-30, GLO-90 and EU-DEM) (ESA, 2025) and products

300 such as DeltaDTM (Pronk et al., 2024) which provide high-resolution topographic and bathymetric data. In addition, global bare-earth elevation data can be obtained from FABDEM, global bare-earth DEM derived from Copernicus GLO-30 (Meadows et al., 2024). LULC data can be drawn from global products such as ESA WorldCover (Zanaga et al., 2022) and building footprints and infrastructure can be obtained from OpenStreetMap data. With these inputs and the approach presented here, coastal managers can assess coastal hazards related to erosion and flooding under current conditions on

305 urbanized and natural barrier islands and evaluate mitigation measures such as vegetation restoration. The sensitivity study may also provide guidance on the interpretation of results in cases where the input and forcing data are of lower than desired quality.

The results of this study add to the evidence base showing that it is now possible to predict morphological changes across all Sallenger (2000) regimes with a single numerical model. For instance, Van der Lugt et al. (2019) showed good skill for cases

310 of barrier-island breaching on Fire Island (New York, USA) and Matanzas Inlet (Florida, USA) but also highlighted that variations in boundary water levels and wave characteristics influenced breach formation and dune response. They also demonstrated that using spatially variable roughness derived from land-cover data improved model skill. Hegermiller et al. (2022) likewise found that representing vegetation roughness improved the timing and extent of breach development. Moreover, Sherwood et al. (2022) provide a thorough overview of the state of morphological modelling up to recent years.

315 Together with our results, these studies indicate that incorporating detailed land-cover-based roughness can significantly improve predictions of morphological response. These findings highlight that parameter settings, roughness, and boundary-forcing conditions can significantly influence the predicted morphological response, underscoring the importance of careful calibration and sensitivity testing when applying XBeach to storm-impact assessments.

5.2 Impact of Supplemental Vegetation on Morphological Response of Vegetated Barrier Island

320 Vegetation influences coastal morphology by affecting hydrodynamic forces and sediment transport processes, as its presence enhances bed roughness, reduces erosion, and promotes sediment deposition (Feagin et al., 2015; Figlus et al., 2014; McGuirk et al., 2022). To evaluate the impact of supplemental vegetation, vegetation patches with a Manning's n value of 0.04 (primary vegetation) were added to Scenario 3, as shown in Fig. 9a, and referred to as Scenario 3a. These patches were placed at elevations above 1 meter relative to the mean sea level (MSL = –0.188 m), and the same vegetation

325 patches were then allowed to evolve into secondary vegetation (Manning's n = 0.05) to investigate what happens if the same vegetation matures over time. Transects 1 and 2 in Fig. 9 (panels b and c) show the effect of vegetation, with Scenario 3a indicating noticeable sediment accumulation within these newly vegetated zones compared to the base case Scenario 3 without the added vegetation strips. The vegetated strips elevated the dune crest by approximately 0.5 m (Fig. 9b) at x = 450 m. Introducing narrow strips of primary vegetation (Fig. 10b) led to sediment accumulation at the breach location and showed that the overwash deposit did not connect to the back barrier over an alongshore distance of 2.8 km. Allowing these

330 same strips to mature into full secondary vegetation (Fig. 10d) resulted in reduced erosion around the vegetated zones alongshore (x ≈ 2.5 km). Additionally, the breach location shifted southward, with increased sedimentation of the breach channel in both cases (shown in blue in Fig. 10c and 10e). Overall, these results demonstrate that vegetation establishment and maturation substantially increase surface roughness and reduce erosion.
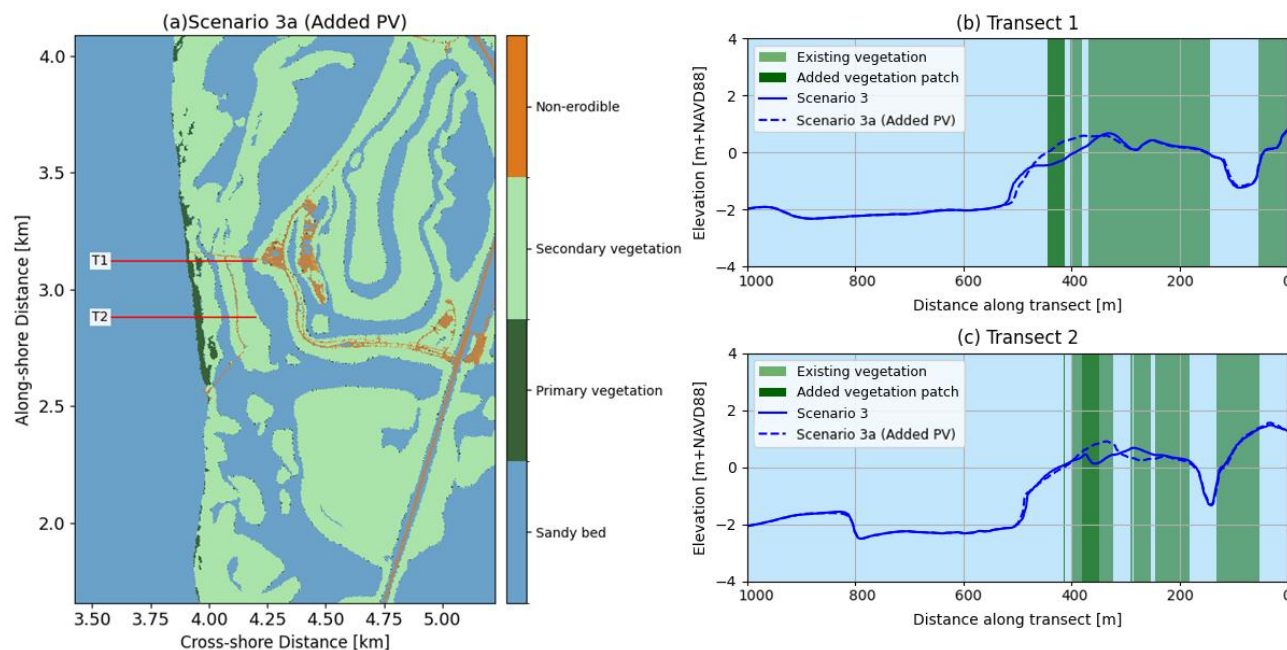
Figure 9 Scenario 3 (based on NOAA LULC dataset) at Lovers Key with (S3a) and without (S3) added primary vegetation (PV). **(a)** Spatial distribution showing sandy bed, primary vegetation, secondary vegetation, and non-erodible areas, with transect locations (T1, T2). **(b–c)** Cross-shore profiles along Transects 1 and 2, comparing Scenario 3 (solid blue) and Scenario 3 with added PV (dashed blue), with existing vegetation (light green) and added patches (dark green).
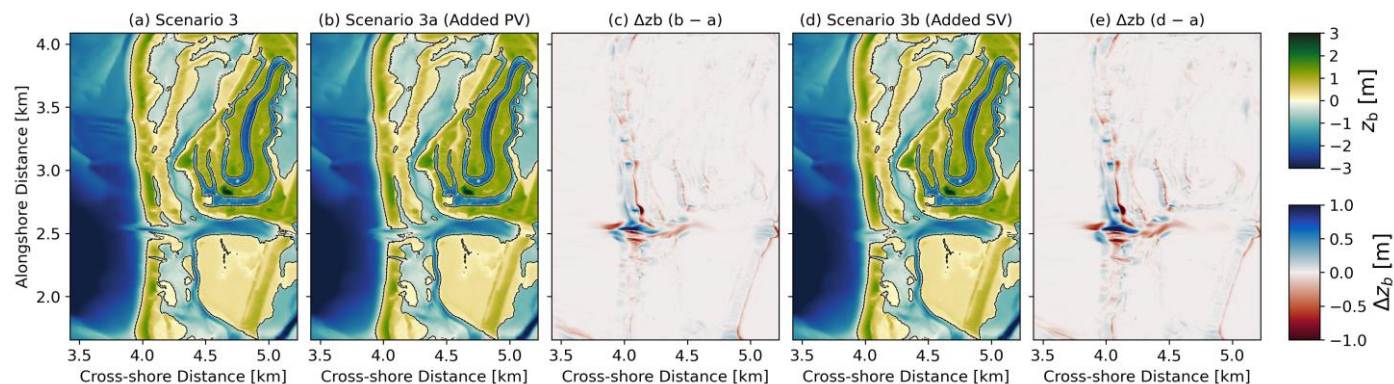
Figure 10 Comparison of Scenario 3 with and without added vegetation at Lovers Key (see Fig. 9): **(a)** Scenario 3, base case based on the NOAA LULC dataset; **(b)** Scenario 3a with added primary vegetation; **(c)** relative change between Scenario 3a and Scenario 3; **(d)** Scenario 3b with added secondary vegetation; and **(e)** relative change between Scenario 3b and Scenario 3. Blue indicates sedimentation and red indicates erosion relative to the base case

6 Conclusions

The effect of vegetation and built environment on the morphodynamic response of the natural Lovers Key barrier island and adjacent urbanized Fort Myers Beach to Hurricane Ian was investigated using observed data (remotely-sensed and in-situ) and the numerical model XBeach with data analysis revealing sedimentation and erosion patterns across both study sites, as

350 well as breach formation and dune crest changes at Lovers Key. Three model scenarios were developed: In Scenario 1, the baseline sandy-bed case, in which vegetation and built environments are not taken into account. Scenario 2 is based on NOPP Land Use and Land Cover (LULC) data, and Scenario 3 uses NOAA LULC data; both incorporate vegetation and built environment s. The modelled results from Scenarios 2 and 3 reproduced the NOAA and FGCU post-Ian observations, capturing erosion and deposition patterns with Brier Skill Scores of 0.38 and 0.40 for Lovers Key, and 0.42 and 0.45 for Fort

355 Myers Beach, which are classified as "reasonable". At Fort Myers Beach, the dense built environment introduced spatial heterogeneity in bed roughness, influencing sediment transport pathways. In contrast, Lovers Key's natural vegetation and dune systems enhanced hydraulic roughness, leading to less erosion. These results highlight that incorporating bed roughness based on LULC data as in Scenarios 2 and 3 vastly improves model performance compared to the uniform sandy-bed case. Sensitivity analyses indicated that variations in Manning's *n* value, wave skewness and asymmetry factor, the morphological

360 acceleration factor, and boundary water levels affected predicted erosion and deposition at both sites, highlighting the model's sensitivity to parameter calibration. The supplemental vegetation analysis showed that introducing and maturing vegetation patches increased bed roughness, reduced dune erosion, and altered breach dynamics under storm conditions. Effective application to other beaches requires high-quality pre- and post-storm elevation data, vegetation and built environment, and reliable boundary forcing data (waves, and surge). With these inputs, models can identify erosion hotspots,

365 forecast overwash and breaching, and test adaptation measures.

Authors Contribution

MHI: Data analysis, numerical modelling, and writing the original draft. AvD: Conceptual development, writing, and editing. DR: Quality control and editing. EQ: Writing and editing. CD: Data provision, writing, and editing.

Competing Interests

370 The authors declare that they have no conflict of interest.

Data Availability Statement

Topographic and bathymetric data were obtained from the NOAA Data Access Viewer https://coast.noaa.gov/dataviewer. Pre-Hurricane Ian topo-bathymetric data is labelled as 2022 USACE NCMP Topo-bathy Lidar DEM: Gulf Coast (FL), and post-Hurricane Ian data as 2022 USACE FEMA Post-Ian Topobathy Lidar DEM: Florida. Land cover datasets include the

375 2022 NOAA C-CAP Version 2 Canopy Cover: Florida and the 2022 NOAA C-CAP Version 2 Impervious Cover: Florida.
The XBeach model (version 1.24.6057-Halloween) was used, accessible at https://oss.deltares.nl/web/xbeach/.

Acknowledgements

We sincerely thank Mr. Michael T. Poff of Coastal Engineering Consultants and the Surveying Team at Florida Gulf Coast
380 University for generously sharing the topo-bathymetric data used in this research. We also acknowledge Deltares for
providing CUDEM 2018 and the Land Use Land Cover data from the National Oceanographic Partnership Program.

Appendix A Sensitivity Analysis of Morphological Response to Model Parameters

The sensitivity of XBeach's morphodynamic predictions to bottom friction values was tested by varying Manning's *n* values
for vegetated areas. Two runs were compared against the baseline Scenario 3 values (primary vegetation, PV, Manning's *n* =
385 0.04; secondary vegetation, SV, Manning's *n* = 0.05): a +10% case (PV = 0.044, SV = 0.055) and a –10% case (PV = 0.036,
SV = 0.045). Increasing Manning's *n* increased friction, which resulted in less dune erosion and landward sediment transport
(red band), as shown in Fig. A1e. Conversely, reducing roughness by 10% amplified dune erosion, with red band indicating
erosion and deposition farther inland (Fig. A1c). These results highlight the role of vegetation in stabilizing coastal features,
as even small changes in roughness can alter sediment redistribution during storms.

390 The wave skewness and asymmetry parameters *facAs*, *facSk*, and *facua* control time-averaged flows driven by wave
asymmetry, skewness, and their combined effects, respectively (*facAs* = 0.20, *facSk* = 0.15, *facua* = 0.175; Roelvink et al.,
2009). Three simulations using Scenario 3's roughness map were performed: the base case (*facua* = 0.175), a lower value
(*facua* = 0.150), and a higher value (*facua* = 0.30). Reducing facua produced light blue band along the dunes (Fig. A2c),
indicating relatively lower crest change and less pronounced landward transport compared to the base case. In contrast, *facua*
395 = 0.30 generated red bands seaward of the dune toe and broader inland blue zones (Fig. A2e), reflecting a relative increase in
crest change and landward redistribution of sediment. These results demonstrate that *facua* is a key parameter in barrier
island response, with modest reductions dampening morphologic change and higher values intensifying it (Van Der Lugt et
al., 2019).

The morphological acceleration factor (*morfac*) of 5 was selected for the final simulations, as tests showed that *morfac* = 3
400 produced very similar spatial patterns but at a higher computational cost, whereas *morfac* = 10 yielded unrealistic
morphodynamic changes. Specifically, with *morfac* = 10 (Fig. A3e), bed-level change was exaggerated, producing greater
erosion, multiple breaches, and wider sediment transport across the island. In contrast, *morfac* = 3 resulted in smoother,
spatially constrained changes that more closely reflected observed patterns (Fig. A3c). These results demonstrate that
excessively high *morfac* values can distort morphodynamic responses, while *morfac* = 5 provides a balance between physical
405 realism and computational efficiency.

Finally, the sensitivity of the model to boundary conditions, including water levels and wave height, was assessed by reducing both by 10% (Fig. A4 and A5). This range was chosen to represent potential uncertainty in forecasted or observed forcing data. Lower water levels produced relatively smaller crest change along the primary dune front and beach (blue band) and decreased landward deposition (red band), while a 10% reduction in wave height had a less pronounced effect.

410 These results highlight that the model is more sensitive to storm surge levels than to offshore wave heights, underscoring the importance of accurate surge estimates in post-storm morphodynamic predictions.
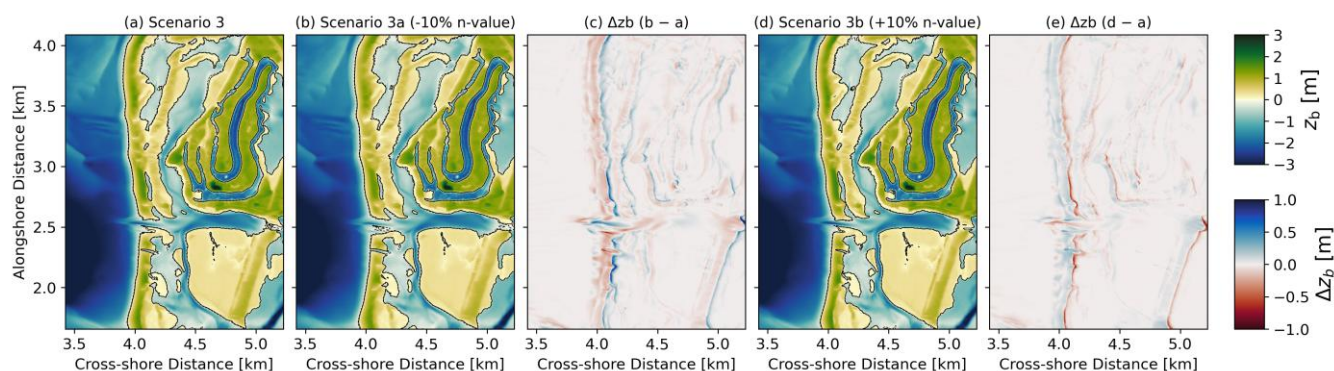
Figure A1 Sensitivity analysis of Manning's roughness coefficient (*n*-values) at Lovers Key: (a) Scenario 3, base case based on the
415 **NOAA LULC dataset; (b) Scenario 3a with a 10% decrease in *n*-value; (c) relative change between Scenario 3a and Scenario 3; (d) Scenario 3b with a 10% increase in *n*-value; and (e) relative change between Scenario 3b and Scenario 3. Blue indicates sedimentation and red indicates erosion relative to the base case**
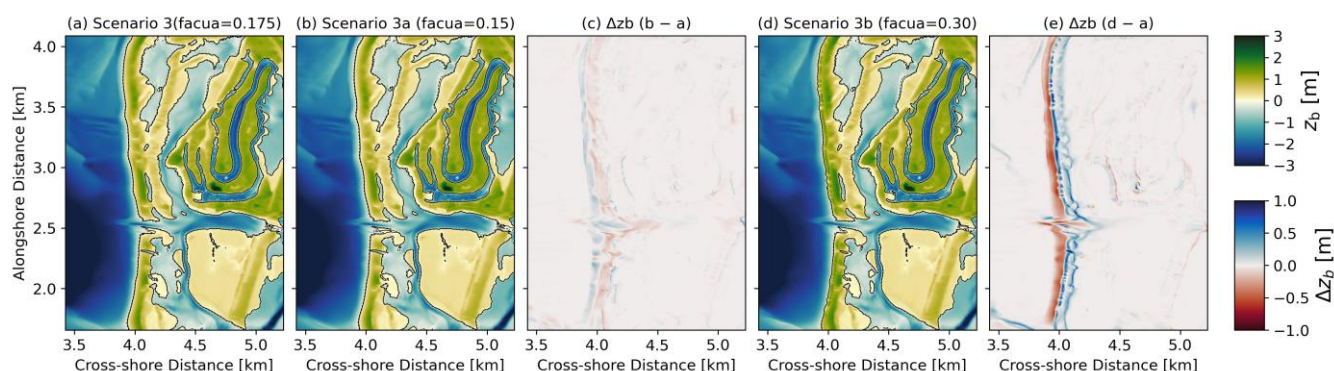
Figure A2 Sensitivity analysis of wave skewness and asymmetry parameter (*facua*) at Lovers Key: (a) Scenario 3, base case with
420 ***facua* = 0.175; (b) Scenario 3a with a decrease in *facua* = 0.15); (c) relative change between Scenario 3a and Scenario 3; (d) Scenario 3b with an increase in *facua*= 0.30; and (e) relative change between Scenario 3b and Scenario 3. Blue indicates sedimentation and red indicates erosion relative to the base case.**
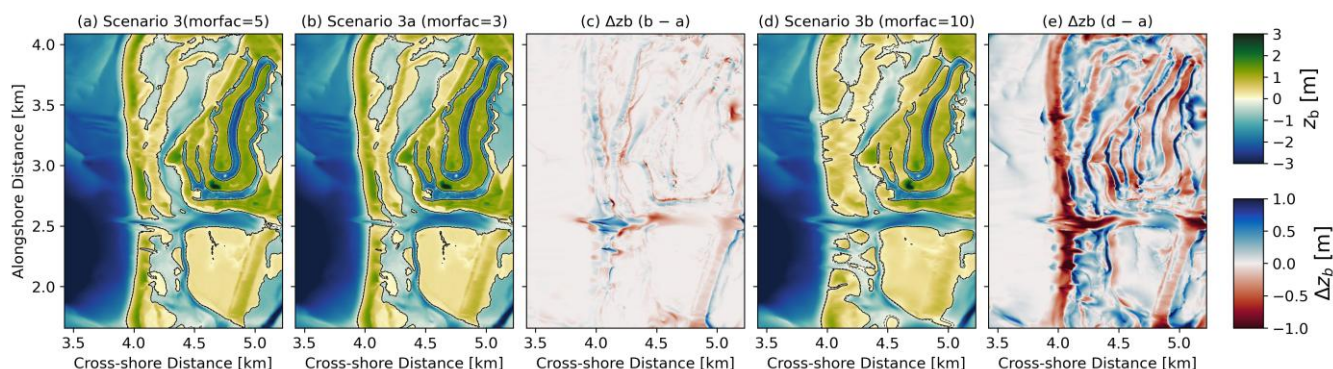
Figure A3 Sensitivity analysis of the morphological acceleration factor (*morfac*) at Lovers Key: (a) Scenario 3, base case with *morfac* = 5; (b) Scenario 3a with a decrease in *morfac* = 3; (c) relative change between Scenario 3a and Scenario 3; (d) Scenario 3b with an increased in *morfac* = 10; and (e) relative change between Scenario 3b and Scenario 3. Blue indicates sedimentation and red indicates erosion relative to the base case.
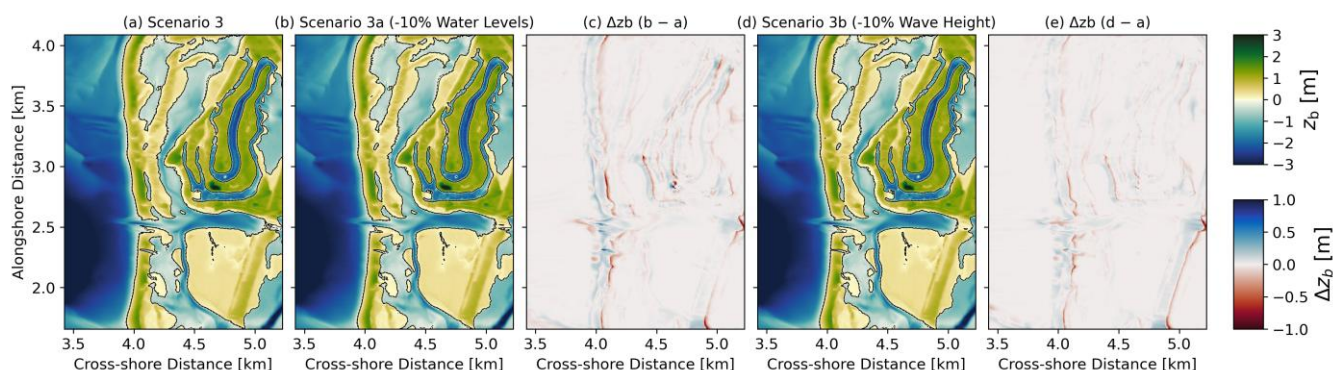
Figure A4 Sensitivity analysis of forcing conditions at Lovers Key: (a) Scenario 3, base case; (b) Scenario 3a with a 10% reduction in water levels; (c) relative change between Scenario 3a and Scenario 3; (d) Scenario 3b with a 10% reduction in wave height; and (e) relative change between Scenario 3b and Scenario 3. Blue indicates sedimentation and red indicates erosion relative to the base case.
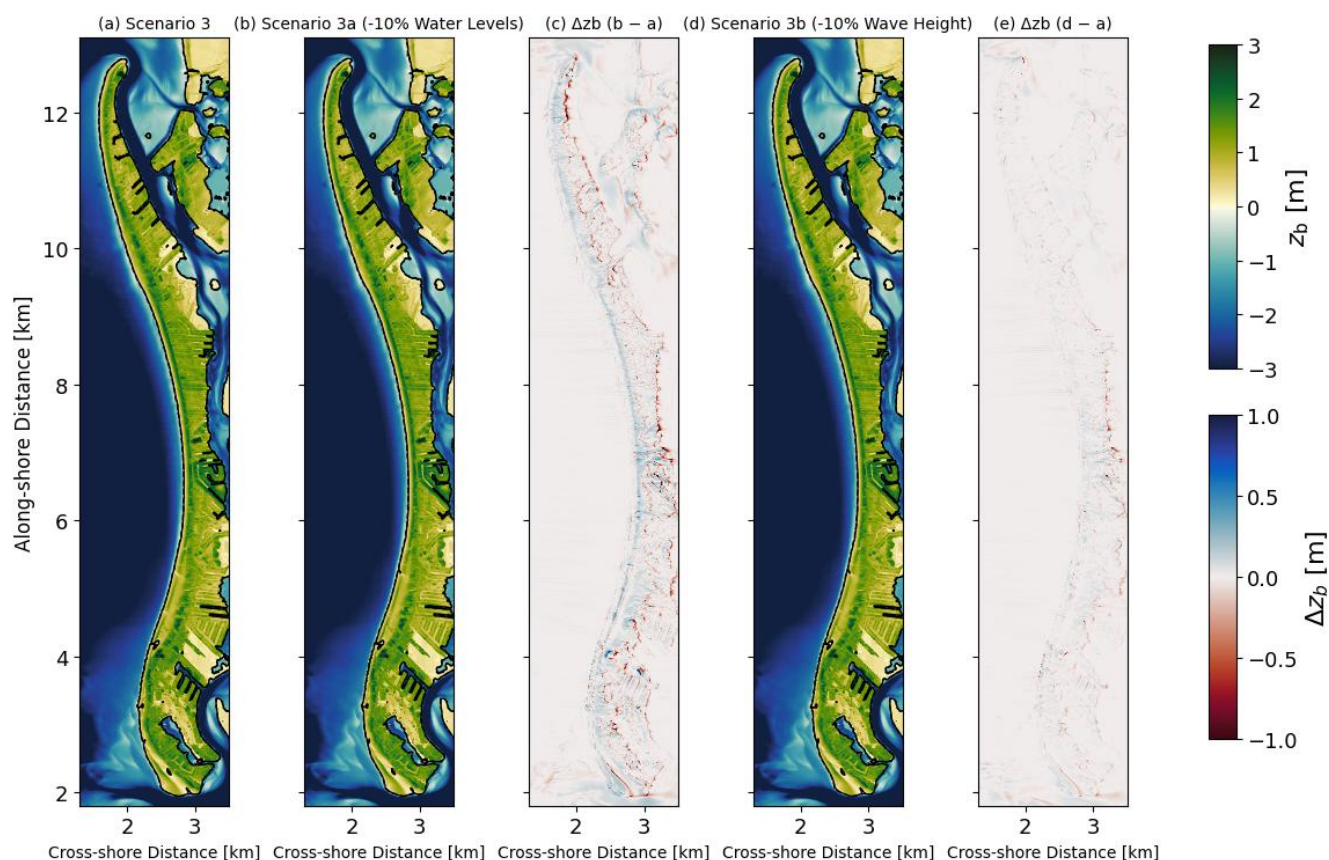
435 **Figure A5 Sensitivity analysis of forcing conditions at Fort Myers Beach: (a) Scenario 3, base case; (b) Scenario 3a with a 10% reduction in water levels; (c) relative change between Scenario 3a and Scenario 3; (d) Scenario 3b with a 10% reduction in wave height; and (e) relative change between Scenario 3b and Scenario 3. Blue indicates sedimentation and red indicates erosion relative to the base case.**

References

440 Almeida, L. P., Vousdoukas, M. V., Ferreira, Ó., Rodrigues, B. A., and Matias, A.: Thresholds for storm impacts on an exposed sandy coastal area in southern Portugal, Geomorphology, 143–144, 3–12, https://doi.org/10.1016/j.geomorph.2011.04.047 , 2012.

Brooks, S. M., Spencer, T., and Christie, E. K.: Storm impacts and shoreline recovery: mechanisms and controls in the southern North Sea, Geomorphology, 283, 48–60, https://doi.org/10.1016/j.geomorph.2017.01.007, 2017.

445 De Vet, P. L. M., McCall, R. T., Den Bieman, J. P., Stive, M. J. F., and Van Ormondt, M.: Modelling dune erosion, overwash and breaching at Fire Island (NY) during Hurricane Sandy, in: Proc. Coastal Sediments 2015, San Diego, USA, July 2015, https://doi.org/10.1142/9789814689977_0006, 2015.

Doyle, J., Hodur, R., Chen, S., Jin, Y., Msokaitis, J., Wang, S., Hendricks, E., Jin, J., and Smith, T.: Tropical cyclone prediction using COAMPS-TC, Oceanography, 27(3), 104–115, https://doi.org/10.5670/oceanog.2014.72, 2014.

450 European Space Agency (ESA): *Copernicus DEM (GLO-30 and GLO-90)*, ESA, available at: https://doi.org/10.5270/ESA-c5d3d65, 2025.

FDEP: Lovers Key State Park approved management plan, Florida Department of Environmental Protection, available at: https://floridadep.gov/parks/parks-office-park_planning/documents/lovers-key-state-par, 2005.

Feagin, R. A., Figlus, J., Zinnert, J. C., Sigren, J., Martínez, M. L., Silva, R., Smith, W. K., Cox, D., Young, D. R., and

455 Carter, G.: Going with the flow or against the grain? The promise of vegetation for protecting beaches, dunes, and barrier islands from erosion, Front. Ecol. Environ., 13(4), 203–210, https://doi.org/10.1890/140218, 2015.

Figlus, J., Sigren, J. M., Armitage, A. R., and Tyler, R. C.: Erosion of vegetated coastal dunes, Coast. Eng. Proc., 1(34), 20, https://doi.org/10.9753/icce.v34.sediment.20, 2014.

FitzGerald, D. M., Fenster, M. S., Argow, B. A., and Buynevich, I. V.: Coastal impacts due to sea-level rise, Annu. Rev.

460 Earth Planet. Sci., 36, 601–647, https://doi.org/10.1146/annurev.earth.35.031306.140139, 2008.

Hapke, C. J., Brenner, O. T., and Henderson, R. E.: Quantifying the geomorphic resiliency of barrier island beaches, in: Proc. Coastal Sediments 2015, San Diego, USA, July 2015, https://doi.org/10.1142/9789814689977_0249, 2015.

Harley, M. D., Turner, I. L., Middleton, J. H., Kinsela, M. A., Hanslow, D., and Mumford, P.: Observations of beach recovery in SE Australia following the June 2016 east coast low, unpublished manuscript, 2017.

465 Harris, L., Nel, R., Smale, M., and Schoeman, D.: Swashed away? Storm impacts on sandy beach macrofaunal communities, Estuar. Coast. Shelf Sci., 94(3), 210–221, https://doi.org/10.1016/j.ecss.2011.06.013, 2011.

Hauptman, L., Mitsova, D., and Briggs, T. R.: Hurricane Ian damage assessment using aerial imagery and LiDAR: a case study of Estero Island, Florida, J. Mar. Sci. Eng., 12(4), 668, https://doi.org/10.3390/jmse12040668, 2024.

Hegermiller, C. A., Warner, J. C., Olabarrieta, M., Sherwood, C. R., and Kalra, T. S.: Modeling of barrier breaching during

470 Hurricanes Sandy and Matthew, J. Geophys. Res.: Earth Surf., 127, e2021JF006307, https://doi.org/10.1029/2021JF006307, 2022.

Houser, C., Hapke, C., and Hamilton, S.: Controls on coastal dune morphology, shoreline erosion and barrier island response to extreme storms, Geomorphology, 100(3–4), 223–240, https://doi.org/10.1016/j.geomorph.2007.12.007, 2008.

IPCC: Global Warming of 1.5°C – SR15, Intergovernmental Panel on Climate Change, available at:

475 http://refhub.elsevier.com/S0272-7714(19)30520-7/sref21, 2018.

IPCC: Climate Change 2021 – The Physical Science Basis: Working Group I Contribution to the Sixth Assessment Report of the Intergovernmental Panel on Climate Change, Cambridge University Press, Cambridge, UK, https://doi.org/10.1017/9781009157896, 2021.

Jiménez, J. A., Gracia, V., Valdemoro, H. I., Mendoza, E. T., and Sánchez-Arcilla, A.: Managing erosion-induced problems

480 in NW Mediterranean urban beaches, Ocean Coast. Manag., 54(12), 907–918, https://doi.org/10.1016/j.ocecoaman.2011.05.003, 2011.

Jiménez, J. A., Sanuy, M., Ballesteros, C., and Valdemoro, H. I.: The Tordera Delta, a hotspot to storm impacts in the coast northwards of Barcelona (NW Mediterranean), Coast. Eng., 134, 148–158, https://doi.org/10.1016/j.coastaleng.2017.08.012, 2018.

485   Lavaud, L., Bertin, X., Martins, K., Arnaud, G., and Bouin, M.-N.: The contribution of short-wave breaking to storm surges: the case Klaus in the southern Bay of Biscay, Ocean Model., 156, 101710, https://doi.org/10.1016/j.ocemod.2020.101710, 2020.

Lazarus, E. D., Goldstein, E. B., Taylor, L. A., and Williams, H. E.: Comparing patterns of hurricane washover into built and unbuilt environments, Earth's Future, 9(3), e2020EF001818, https://doi.org/10.1029/2020EF001818, 2021.

490   Lindemer, C. A., Plant, N. G., Puleo, J. A., Thompson, D. M., and Wamsley, T. V.: Numerical simulation of a low-lying barrier island's morphological response to Hurricane Katrina, Coast. Eng., 57(11–12), 985–995, https://doi.org/10.1016/j.coastaleng.2010.06.004, 2010.

Mattocks, C. and Forbes, C.: A real-time, event-triggered storm surge forecasting system for the state of North Carolina, Ocean Model., 25(3–4), 95–119, https://doi.org/10.1016/j.ocemod.2008.06.008, 2008.

495   McCall, R. T., Van Thiel de Vries, J. S. M., Plant, N. G., Van Dongeren, A. R., Roelvink, J. A., Thompson, D. M., and Reniers, A. J. H. M.: Two-dimensional time-dependent hurricane overwash and erosion modeling at Santa Rosa Island, Coast. Eng., 57(7), 668–683, https://doi.org/10.1016/j.coastaleng.2010.02.006, 2010.

McGuirk, M. T., Kennedy, D. M., and Konlechner, T.: The role of vegetation in incipient dune and foredune development and morphology: a review, J. Coast. Res., 38(2), https://doi.org/10.2112/JCOASTRES-D-21-00021.1, 2022.

500   NOAA: Continuously updated digital elevation model (CUDEM) – Ninth arc-second resolution bathymetric-topographic tiles, NOAA Natl. Cent. Environ. Inf. [data set], https://chs.coast.noaa.gov/htdata/raster2/elevation/NCEI_ninth_Topobathy_2014_8483/FL/, 2018.

NOPP: National Oceanographic Partnership Program – NHCI Task 1 (Gesch), NOAA Natl. Cent. Environ. Inf. [data set], https://nopphurricane.sofarocean.com/updates/task-1-p-i-gesch, 2021.

505   Nordstrom, K. F.: Reestablishing naturally functioning dunes on developed coasts, Environ. Manag., 25(1), 37–51, https://doi.org/10.1007/s002679910004 , 2000.

OCM Partners: 2022 USACE FEMA Post Ian Topobathy LiDAR DEM: Florida from 2022-01-01 to 2022-12-31, NOAA Natl. Cent. Environ. Inf. [data set], https://www.fisheries.noaa.gov/inport/item/71740, 2025b.

OCM Partners: 2022 USACE NCMP Topobathy LiDAR DEM: Gulf Coast (FL) from 2022-01-01 to 2022-12-31, NOAA
510   Natl. Cent. Environ. Inf. [data set], https://www.fisheries.noaa.gov/inport/item/71772 , 2025a.

Office for Coastal Management: 2020–2023 CCAP Version 2 Canopy Cover, NOAA Natl. Cent. Environ. Inf. [data set], https://www.fisheries.noaa.gov/inport/item/70562, 2025b.

Office for Coastal Management: 2020–2023 CCAP Version 2 Impervious Cover, NOAA Natl. Cent. Environ. Inf. [data set], https://www.fisheries.noaa.gov/inport/item/70563, 2025a.

515 Pardo-Pascual, J. E., Almonacid-Caballer, J., Ruiz, L. A., Palomar-Vázquez, J., and Rodrigo-Alemany, R.: Evaluation of storm impact on sandy beaches of the Gulf of Valencia using Landsat imagery series, Geomorphology, 214, 388–401, https://doi.org/10.1016/j.geomorph.2014.02.020, 2014.

Passeri, D. L., Long, J. W., Plant, N. G., Bilskie, M. V., and Hagen, S. C.: The influence of bed friction variability due to land cover on storm-driven barrier island morphodynamics, Coast. Eng., 132, 82–94,
520 https://doi.org/10.1016/j.coastaleng.2017.11.005, 2018.

Pronk, M., Hooijer, A., Eilander, D., Haag, A., de Jong, T., Vousdoukas, M., and Eleveld, M.: DeltaDTM: A global coastal digital terrain model, *Sci. Data*, 11, 273, https://doi.org/10.1038/s41597-024-02926-4, 2024.

Roelvink, D., Reniers, A., Van Dongeren, A., Van Thiel de Vries, J., McCall, R., and Lescinski, J.: Modelling storm impacts on beaches, dunes and barrier islands, Coast. Eng., 56(11–12), 1133–1152, https://doi.org/10.1016/j.coastaleng.2009.08.006,
525 2009.

Salgado, S. C.: Predicting erosion of vegetated dunes during hurricanes, Master's thesis, Delft University of Technology, available at: https://resolver.tudelft.nl/uuid:96076fda-d0c7-450e-951d-b62d0f3675bf, 2023.

Sallenger, A. H.: Storm impact scale for barrier islands, J. Coast. Res., 16, 2000.

Sherwood, C. R., Van Dongeren, A., Doyle, J., Hegermiller, C. A., Hsu, T.-J., Kalra, T. S., Olabarrieta, M., Penko, A. M.,
530 Rafati, Y., Roelvink, D., Van der Lugt, M., Veeramony, J., and Warner, J. C.: Modeling the morphodynamics of coastal responses to extreme events: what shape are we in?, Annu. Rev. Mar. Sci., 14(1), 457–492, https://doi.org/10.1146/annurev-marine-032221-090215, 2022.

Stutz, M. L. and Pilkey, O. H.: Open-ocean barrier islands: global influence of climatic, oceanographic, and depositional settings, J. Coast. Res., 272, 207–222, https://doi.org/10.2112/09-1190.1, 2011.

535 Tebaldi, C., Strauss, B. H., and Zervas, C. E.: Modelling sea-level rise impacts on storm surges along US coasts, Environ. Res. Lett., 7(1), 014032, https://doi.org/10.1088/1748-9326/7/1/014032, 2012.

Van der Lugt, M. A., Quataert, E., Van Dongeren, A., Van Ormondt, M., and Sherwood, C. R.: Morphodynamic modeling of the response of two barrier islands to Atlantic hurricane forcing, Estuar. Coast. Shelf Sci., 229, 106404, https://doi.org/10.1016/j.ecss.2019.106404, 2019.

540 Van Puijenbroek, M. E. B., Nolet, C., De Groot, A. V., Suomalainen, J. M., Riksen, M. J. P. M., Berendse, F., and Limpens, J.: Exploring the contributions of vegetation and dune size to early dune development using unmanned aerial vehicle (UAV) imaging, Biogeosciences, 14(23), 5533–5549, https://doi.org/10.5194/bg-14-5533-2017 , 2017.

Van Rijn, L. C., Walstra, D. J. R., Grasmeijer, B., Sutherland, J., Pan, S., and Sierra, J. P.: The predictability of cross-shore bed evolution of sandy beaches at the time scale of storms and seasons using process-based profile models, Coast. Eng.,
545 47(3), 295–327, https://doi.org/10.1016/S0378-3839(02)00120-5, 2003.

Zanaga, D., Van de Kerchove, R., Daems, D., De Keersmaecker, W., Brockmann, C., Kirches, G., Bontempi, I., Cartus, O., Santoro, M., and Arino, O.: ESA WorldCover 10 m 2021, version v200, European Space Agency [data set], https://doi.org/10.5281/zenodo.7254221, 2022.